ACS APPLIED MATERIALS & INTERFACES

Research Article

www.acsami.org

Reduced Graphene Oxide/ZnO Composite: Reusable Adsorbent for Pollutant Management

Jinfeng Wang,[†] Takuya Tsuzuki,[†] Bin Tang,[†] Xueliang Hou,[†] Lu Sun,*[,†] and Xungai Wang*[,†,‡]

[†]Institute for Frontier Materials, Deakin University, Geelong, Victoria, Australia 3217

[‡]Ministry of Education Key Laboratory for Textile Fibers and Products, Wuhan Textile University, Wuhan, China

Supporting Information

ABSTRACT: Reduced graphene oxide (RGO) coated with ZnO nanoparticles (NPs) was synthesized by a self-assembly and in situ photoreduction method, and then their application for removing organic pollutant from water was investigated. The RGO@ZnO composite nanomaterial has unique structural features including well-dispersed NPs on the surface and dense NPs loading. This composite exhibited a greatly improved Rhodamine B (RhB) adsorption capacity and an improved photocatalytic activity for degrading RhB compared to neat ZnO NPs. These properties made RGO@ZnO reusable for pollutant adsorbent. The composite showed an excellent cycling performance for organic pollutant removal up to 99% recovery over several cycles via simulated sunlight irradiation.

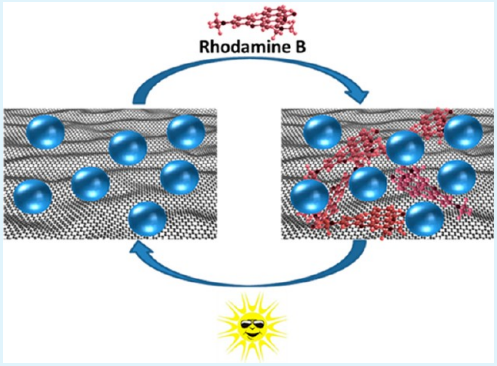

KEYWORDS: *graphene, photoreduction, pollutant removal, recovery, photocatalytic activity*

1. INTRODUCTION

Aromatic pollutants are widely found in the effluents from the dyestuff, pesticide, petrochemical, and other industries. Because of their high solubility in water, they can be easily transported to environment and may cause serious problems to our health. Many studies have focused on the efficient elimination of the organic pollutants by using adsorbents. However, for most of the conventional adsorbents, the adsorption properties are not recoverable. It is important to develop new reusable adsorbents with high adsorption capacities for the management of aromatic pollutant.

The high surface area of nanomaterial brings new prospects to the pollutant management. For example, graphene has a very large theoretical surface area (2620 $m^2\ g^{-1}$) with potential low manufacturing cost. This attribute makes graphene a promising adsorbent for practical applications in environmental pollutant management.[1−3] However, it is generally difficult to maintain the large surface area of graphene because of the strong van der Waals interaction between them.[4] One effective method to obtain graphene as individual sheet in suspension is to functionalize the surface of graphene sheets with NPs. The existence of inorganic particles on the graphene surface can prevent the aggregation of graphene sheets and retain the surface area at a high level. Therefore, it is reasonable to believe that graphene-based semiconductor NPs composites like graphene/ZnO can be obtained with a large surface area and be used as pollutant adsorbent for environmental application.

Many efforts have been devoted to obtaining metal[5−7] or metal oxide[8−10] NPs with graphene by reduction of exfoliated graphene oxide (GO). However, the reduction of GO often relies on toxic reducing agents such as hydrazine or on high temperature treatment with the formation of interface bonds between inorganic and carbon-based phase.[11] In contrast, photocatalytic reduction of GO is now accepted as an environmentally friendly and energy-efficient method for the production of RGO.[12−15] Photocatalytic reduction of GO has been applied in fabricating graphene based composites using semiconductor oxides, typically TiO_2 and ZnO. Williams et al.[12,13] and Liu et al.[16] fabricated composites of graphene and ZnO or TiO_2 by carrying out photocatalytic reduction. Ng et al.[17,18] synthesized the composites of graphene and TiO_2, WO_3, or $BiVO_4$ via a one-step UV or visible light induced-photocatalytic reduction process and they exhibited higher photoelectrocatalytic efficiency than their parent materials.

It is an important factor for pollutant absorbent to be reusable. In the case of graphene/ZnO, it requires strong interaction between graphene and ZnO NPs to preserve the composite structure after several recycles. Yang et al.[19] reported that most graphene/ZnO composites were fabricated using simple mixing method, and the loading capacity was limited because of the weak interaction between ZnO and graphene. Therefore, they combined zinc ions with carbon materials using poly (vinyl pyrrolidone) (PVP) as an intermediate to anchor ZnO NPs on the functionalized graphene sheets after a heating annealing process, and got a higher loading level compared with graphene/ZnO composites without PVP. Furthermore, PVP

Received: March 12, 2012
Accepted: June 7, 2012
Published: June 7, 2012

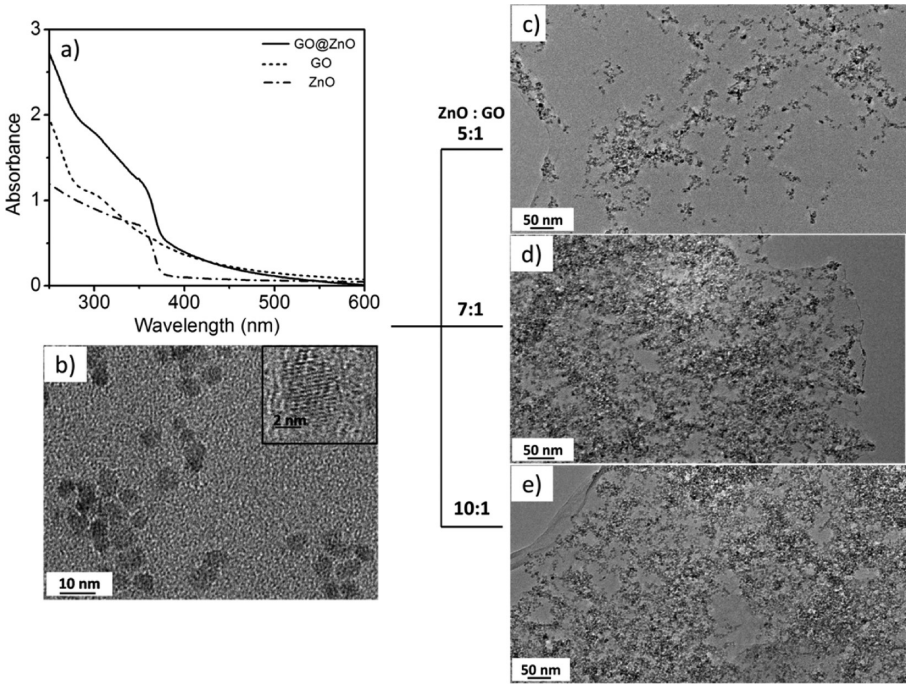

Figure 1. (a) UV−vis absorption spectra of GO@ZnO, GO and PVP-capped ZnO aqueous suspensions. TEM images of (b) PVP-capped ZnO NPs, and (c−e) GO@ZnO prepared with PVP-capped ZnO to GO volume ratio of 5:1, 7:1, and 10:1, respectively.

can be adsorbed onto a broad range of materials such as metals (e.g., gold, silver, iron), metal oxides (e. g., kaolinite, TiO_2, iron oxide, alumina),[20] silica,[21] and graphite.[22] It stabilizes colloidal particles in water and many nonaqueous solvents. PVP also shows great affinity to GO and RGO surface via hydrophobic interaction between PVP chains and sp^2-carbon conjugate structures on GO and RGO.[9,23] Hence the use of PVP as an intermediate is expected to increase the loading of ZnO NPs on graphene and preserve the graphene/ZnO structure after several recycled usage.

In this article, we demonstrate the fabrication of RGO@ZnO using self-assembly method. ZnO NPs were loaded on the surface of GO nanosheets using PVP as the intermedium without further treatment and a subsequent in situ photoreduction procedure converted GO to RGO due to the photocatalytic activity of ZnO NPs. In this way, RGO@ZnO with dense loading of ZnO NPs was fabricated and the reusable application of RGO@ZnO as the pollutant adsorbent was investigated. The hydrophilic surface of ZnO NPs helped the dispersion of RGO@ZnO in water for effective adsorption of water-soluble pollutants. Also the high density of PVP-capped ZnO NPs assisted the facile separation of RGO@ZnO from water after adsorption by sedimentation or centrifugation. More importantly, because of the photocatalytic activity of ZnO NPs, the organic pollutant adsorbed on RGO@ZnO can be degraded by ZnO NPs under simulated sunlight irradiation, resulting in a recovered adsorption capacity of RGO@ZnO.

2. EXPERIMENTAL SECTION

2.1. Synthesis of PVP-Capped ZnO NPs. First, 0.27 g of zinc acetate was dissolved in ethanol and heated to 60 °C under constant stirring for 2 h. Then, 0.50 g of PVP was added to the solution. After the PVP was dissolved in ethanol, the solution was cooled to room temperature. A sodium hydroxide solution was prepared separately by dissolving 0.098 g of sodium hydroxide in 50 mL of ethanol at room temperature in an ultrasonic bath. The sodium hydroxide solution was added dropwise into the zinc acetate solution under constant stirring to form PVP-capped ZnO NPs. The solution mixture was then stirred continuously at 60 °C for up to 2 h. The PVP-capped ZnO particles were flocculated from ethanol via the addition of hexane (30 mL of hexane/10 mL of reaction mixture) and subsequently collected by centrifugation at 6000 rpm for 10 min.

2.2. Preparation of GO Dispersion. GO was prepared using a modified Hummers method.[24] Briefly, 10 g graphite flake and 7.5 g sodium nitrate were added to 300 mL of sulfuric acid (98%), and then 40 g of potassium permanganate was added to the reaction slowly in 1 h. The mixture was stirred at room temperature for 3 days. One L of hydrogen peroxide solution (1% in water) was then added into the mixture. Subsequently, the mixture was filtered and washed with deionized water until pH 7. The resulting black cake was redispersed in deionized water to give a dark brown dispersion, which was subjected to dialysis for 1 week to remove the residual salts and acids. And the brown suspension was dried at 40 °C under vacuum. GO suspension was then obtained by sonicating the as-prepared black solid in water under ambient condition for 30 min. The resulting homogeneous brown dispersion was tested to be stable for several months and used for reduction.

2.3. Self-Assembly of PVP-Capped ZnO NPs with GO Nanosheets. GO nanosheets were used to load PVP-capped ZnO NPs for the production of GO@ZnO hybrids via a simple route at room temperature. Briefly, 7.0 mL of PVP-capped ZnO aqueous dispersion (0.15 mg/mL) was added to 1.0 mL aqueous dispersion of GO with a concentration of 0.5 mg/mL. The mixture of these dispersions was stirred for 20 min to ensure the full contact between the PVP-capped ZnO and GO nanosheets. Then, 6.0 mL of NaCl aqueous solution (1.0 M) were added to the above mixture to flocculate GO@ZnO from the aqueous dispersion. The resulting deposition was subsequently separated by centrifugation, rinsed by deionized water and finally collected after centrifugation.

2.4. Reduction of GO@ZnO to RGO@ZnO by UV irradiation. The deposition collected in the last step was redispersed in water. The water suspension of the composite was exposed to UV light (λ > 300 nm) using a 150 W Oriel xenon arc lamp and a copper sulfate filter for 10 min. The final product was then separated from dispersion by centrifugation at 7000 rpm for 10 min and collected for further characterization.

2.5. Characterization. X-ray diffraction (XRD) data were obtained on a PANalytical's X'Pert Power X-ray Diffraction (40 kV, 30 mA) with Cu−Kα radiation at a scanning rate of 2.4° min^{-1}. The morphologies and structures of the samples were investigated by transmission electron microscopy (TEM) on a JEOL-2100 with an acceleration voltage of 200 kV. X-ray photoelectron spectroscopy (XPS) data were collected on a VG ESCALAB 220-iXL spectrometer with a monochromatic Al−Kα source (1486.6 eV) at 150 W (15 kV, 10 mA). Survey scans were taken at analyzer pass energy of 160 eV. The optical absorption spectra of the samples were obtained using a Varian Cary 3E ultraviolet visible (UV−vis) spectrophotometer. Simulated sunlight tests were carried out using an Atlas Suntest CPS1 instrument equipped with 150 W xenon lamp and a filter (coated quartz dish). Fourier transform infrared (FTIR) spectra were measured with a Bruker Vertex 70 FT-IR spectrophotometer using the KBr method.

2.6. Dye Adsorption and Photocatalytic Activity Test. Dried powder of PVP-capped ZnO and uncapped ZnO NPs was separately dispersed in 50 mL of RhB aqueous solution. The amount of the PVP-capped ZnO and uncapped ZnO NPs was chosen so as to have 4.0 mg/mL of net ZnO in the RhB solution for both cases. The suspensions were stirred for 1 h in the dark to achieve the adsorption and desorption equilibration. Then the UV−vis spectrum of each RhB suspension was measured.

RhB was used as a probe molecule to evaluate the photocatalytic activity of PVP-capped ZnO NPs and RGO@ZnO in response to simulated sunlight irradiation. The characteristic optical absorption peak of RhB at 554 nm was chosen to monitor the photocatalytic degradation process. The experiment was carried out according to the following procedure: dried powder of PVP-capped ZnO NPs and RGO@ZnO was dispersed in 50 mL of RhB aqueous solution with a concentration of 6 ppm in a 100 mL beaker (for all photodegredation experiments, the net amount of ZnO was maintained to be 4.0 mg/mL). The suspension was stirred in the dark for 1 h to ensure the establishment of adsorption and desorption equilibrium of RhB dye molecules on the surface of the above catalysts. Subsequently the suspension was irradiated with simulated sunlight (including both UV and visible light). The flux intensity was 300 W/m^2. At given intervals, 3 mL of the suspension was extracted and then centrifuged at 6000 rpm for 10 min to separate the catalysts from the supernatant. UV−vis absorbance spectra of the supernatant were measured with a spectrophotometer.

3. RESULTS AND DISCUSSION

3.1. Assembly of GO@ZnO. PVP-capped ZnO NPs were synthesized first, and then a simple self-assembly method was used to load ZnO NPs onto GO nanosheets using PVP as the intermedium. PVP-capped ZnO NPs and GO both show characteristic absorption in the UV−vis region, as presented in Figure 1a. One absorption band of GO appears at 300 nm, while the absorption of PVP-capped ZnO is located at 354 nm. Therefore, it is easy to monitor the formation of GO@ZnO by UV−vis spectroscopy, according to the final composite absorbance at the characteristic absorption bands of GO and ZnO. After being washed and redispersed in water, the GO@ZnO showed a broad UV−vis absorption range from 225 to 550 nm. The spectrum of GO@ZnO appears to comprise the spectra from both GO and PVP-capped ZnO,[25] which suggested the coexistence of GO and PVP-capped ZnO NPs in the obtained GO@ZnO. The morphologies of the samples before and after the assembly process were determined by TEM. As shown in Figure 1b, the typical TEM image of PVP-capped ZnO NPs shows all the NPs are nearly spherical in shape. These as-prepared ZnO NPs capped by PVP molecules showed high dispersion stability in water and ethanol (data not shown), which can be ascribed to the strong coordination interaction between ZnO NPs and PVP molecules.[26] Close examination of TEM images (Figure 1c−e) reveals that PVP-capped ZnO NPs were adsorbed on the surface of GO sheets after the assembly process, and almost no free PVP-capped ZnO NPs were found outside of GO sheets. As the ratio of PVP-capped ZnO NPs to GO nanosheets increased from 5:1 to 7:1, the density of PVP-capped ZnO NPs on the surface of GO nanosheets increased (Figure 1c and 1d). Further increase of PVP-capped ZnO to GO ratio from 7:1 to 10:1 resulted in a similarly dense packing of PVP-capped ZnO NPs as shown in Figure 1d and e. Both the UV−vis spectra and TEM results of the GO@ZnO suggested that effective assembly of PVP-capped ZnO NPs on GO nanosheets. To calculate the amount of ZnO loaded on GO, thermogravimetric analysis (TGA) was performed on GO@ZnO (7:1) under an air flow from 50 to 700 °C to remove PVP and GO (see Figure S1 in the Supporting Information). The residual weight ratio was found to be 52.5%, which is considered to be the content of ZnO in GO@ZnO. This loading level of GO@ZnO with PVP as intermedium is much higher compared to that of GO@ZnO without PVP as reported.[19] This also indicates that interaction between PVP and GO assists the assembling of the PVP-capped ZnO NPs on GO nanosheets.

3.2. Reduction of GO@ZnO. The reduction of GO@ZnO to RGO@ZnO was attempted by in situ UV irradiation using the photocatalytic activity of ZnO NPs. In the XPS of the GO@ZnO before and after UV irradiation (see Figure S2 in the Supporting Information), the peaks located at 284.6 eV, 399.2 eV, 531.8 and 1020.8 eV are assigned to the characteristic peaks of C1s, N1s, O1s and Zn 2p, respectively. The atomic percentage ratio of GO@ZnO between element O and Zn decreased after the UV irradiation treatment, which indicates the reduction of GO@ZnO (see Table S1 in Supporting Information). The reduction of the oxygen-containing groups of GO before and after the UV irradiation treatment are further shown in Figure 2. The C 1s XPS spectrum of GO indicates GO with three main components that corresponds to the carbon atoms in different functional groups: the nonoxygenated C−C bond (284.6 eV), the C−O bond (epoxy and hydroxyl) (286.6 eV), and the carboxylate C═O from carboxylic acid

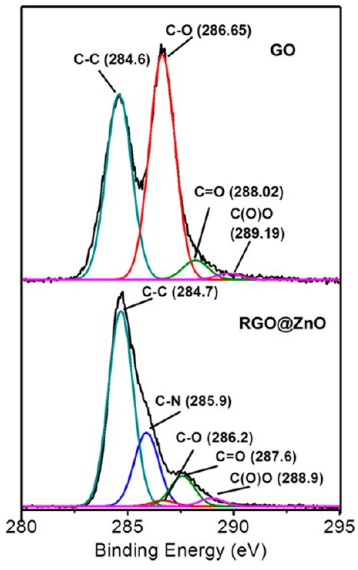

Figure 2. X-ray photoelectron spectroscopy high resolution curves of C 1S of GO alone and RGO@ZnO.

(288.0 eV). After UV irradiation treatment of GO@ZnO, the peak intensity of C−O bonds decreased dramatically and became significantly weak as compared to that of C−C bond, indicating that a considerable degree of oxygen-containing groups of GO@ZnO was reduced by UV irradiation.[12]

The mechanisms of photoreduction in the system of GO and semiconductor NPs such as TiO_2 and ZnO have been proposed earlier.[12,13] Under the irradiation of UV light, the electrons of ZnO NPs are excited, which leads to the electron−hole separation. The electrons trapped in ZnO NPs transfer to GO nanosheets, resulting in the reduction of GO. Because activated tert-amide groups of PVP can only be attacked by the epoxide or hydroxyl groups of GO at acid conditions,[27] and the UV-induced reduction was carried out at pH-neutral conditions, we suggested that PVP did not cause the reduction of GO functional groups.

The reduction from GO@ZnO to RGO@ZnO was further characterized by XRD (Figure 3a) and FTIR (Figure 3b). It can

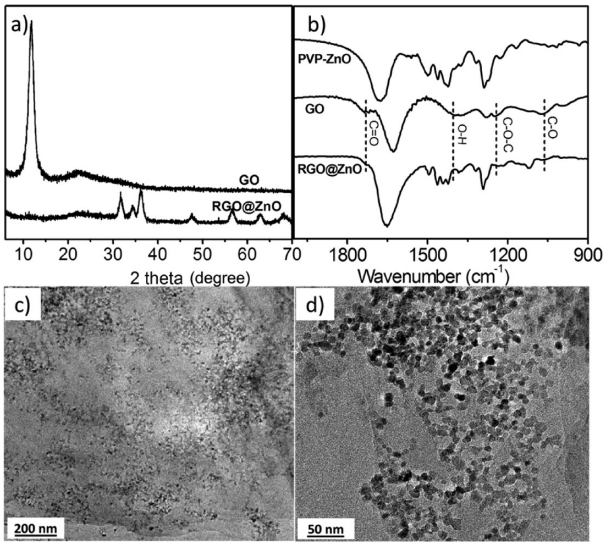

Figure 3. (a) XRD patterns of GO and RGO@ZnO powder. (b) FTIR of PVP-capped ZnO, GO, GO@ZnO, and RGO@ZnO. (c, d) TEM images of RGO@ZnO, which was obtained from in situ photoreduction of GO@ZnO.

be found that GO has a diffraction peak at 2θ = 11.8°, corresponding to a C (002) interplanar spacing of 7.5 Å (Figure 3a). However, this peak disappeared for RGO@ZnO, which indicates the disordered stacking of RGO was formed in the composite. It also supports the conclusion that PVP-capped ZnO NPs were successfully adsorbed on the surface of RGO nanosheets, which prevented the stacking of RGO nanosheets. Moreover, a typical pattern of hexagonal phase Wurtzite ZnO was identified in the curve of RGO@ZnO (JCPDS card, No. 89−0511), which implies that the crystalline structure of ZnO was retained after the UV irradiation treatment. From the FTIR spectra, it can be seen that the characteristic absorption bands of oxide groups in GO, such as C═O stretching vibration peak at 1731 cm^{-1}, the vibration and deformation peaks of O−H groups at 1471 cm^{-1}, the C−O (alkoxy) stretching peak at 1051 cm^{-1}, and the C−O (epoxy) stretching peak at 1243 cm^{-1} decreased dramatically, and some of them disappeared entirely after the reduction treatment, indicating that most oxygen-containing functional groups in the GO were removed.[28,29] This feature further proves the reduction of GO, which is consistent with results of XPS and XRD data.

TEM images of the final RGO@ZnO are shown in Figure 3c and d. Both of the pictures show that PVP-capped ZnO NPs remained densely coated on the surface of GO after the UV irradiation treatment. The fact that PVP-capped ZnO NPs can be well-preserved on the surface of RGO nanosheets after extensive rinsing and centrifugation implied strong binding between and RGO nanosheets, which indicates the intermediating effect of PVP between ZnO NPs and RGO nanosheets.[9]

3.3. Recoverable Adsorption Capacity of RGO@ZnO. Considering the structure of the packed sp^2-bonded carbon atoms of RGO, it is expected that the RGO@ZnO will adsorb delocalized π-bond of the organic aromatic compounds in aqueous solutions. Once adsorbed, the organic compound could be degraded by the photocatalytic activity of ZnO NPs under simulated sunlight irradiation to recover the adsorption capacity of RGO@ZnO. Therefore, the potential of synthesized RGO@ZnO as a reusable organic pollutant scavenger was studied. Herein, a common dye RhB was used as a model organic pollutant.

The dye adsorption capacity of RGO@ZnO (ratio of PVP-capped ZnO:GO was 7:1) was investigated by comparing with that of PVP-capped ZnO NPs. PVP has negligible influence on the dye adsorption process because both PVP-capped and uncapped ZnO showed near identical adsorption characteristics toward RhB under the same conditions (see Figure S3 in the Supporting Information). After the same amount of PVP-capped ZnO and RGO@ZnO was dispersed into RhB solutions, the suspensions were stirred for 1 h in the dark to achieve the adsorption and desorption equilibration. Then the UV−vis optical absorption of each RhB suspension was measured as shown in Figure 4a. The optical absorption intensity of RhB decreased slightly in the presence of PVP-capped ZnO NPs. While in the presence of RGO@ZnO, the absorption intensity became almost 4 times lower than that in the presence of PVP-capped ZnO NPs. This indicates that RGO@ZnO showed 4 times higher dye adsorption capacity than PVP-capped ZnO under the same conditions. The adsorption isotherm of RhB as a function of RhB concentration on RGO@ZnO was shown in Figure 4b and the maximum adsorption capacity (Q_{max}) of RGO@ZnO was found to be 32.6 mg/g. Although the adsorption capacity of RGO@ZnO is similar or lower compared with that of Cu_2O@RGO and Ni@RGO system as reported,[7,10] the photocatalytic activity of ZnO has the advantage to degrade the adsorbed dye under simulated sunlight, and recover the adsorption property of RGO@ZnO.

The reusability of RGO@ZnO was investigated by performing several adsorption and sunlight irradiation cycles (see Figure S4 in the Supporting Information). In each cycle, after RhB was adsorbed by RGO@ZnO, simulated sunlight was irradiated for 20 min at room temperature. As shown in Figure 4c, after the first cycle of adsorption and sunlight irradiation, 78% of the adsorption capacity of RGO@ZnO was recovered. After 4 cycles, the adsorption ability of RGO@ZnO was retained at 77% of the original value. Without irradiation, the adsorption capacity of RGO@ZnO decreased down to 48% of the original value after fourth cycle. Therefore, the irradiation of the simulated sunlight was effective to recover the adsorption efficiency of RGO@ZnO. TEM image of RGO@ZnO after fourth cycle shows that ZnO NPs distributed uniformly on the surface of RGO nanosheets (see Figure S5 in the Supporting Information). The relatively dense and stable packing of ZnO

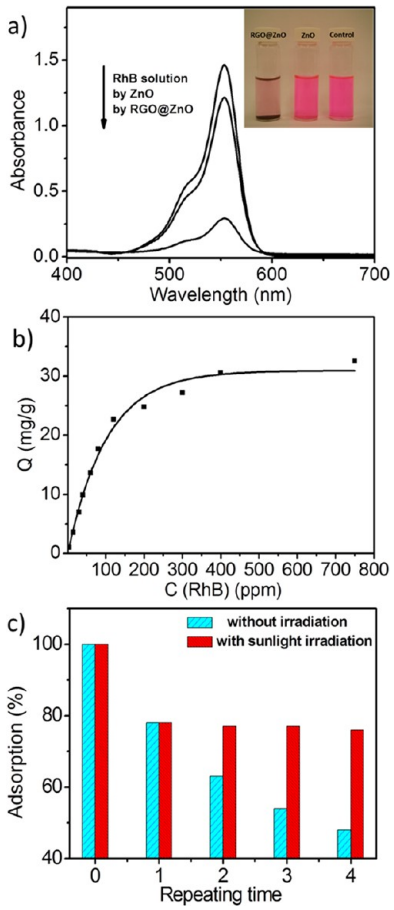

Figure 4. (a) UV−vis absorption spectra of original Rhodamine B (RhB) solution, adsorptive RhB solutions in the presence of PVP-capped ZnO and RGO@ZnO. Insets are images of the original RhB solution, adsorptive RhB solutions in the presence of PVP-capped ZnO and RGO@ZnO. (b) Dye adsorption isotherms of RhB on RGO@ZnO. m/V (concentration for RGO@ZnO) = 4 mg/mL C $(RhB)_{initial}$ = 4−750 ppm, T = 293K. (c) Dye adsorption efficiency of RGO@ZnO with and without sunlight irradiation after several sequential cycles (RhB, 6 ppm; RGO@ZnO, 4 mg/mL).

NPs on the surface of the RGO layers provides the effective photocatalytic degradation of dye molecules on RGO surface, which facilitated the excellent cycling performance of RGO@ZnO. The photocatalytic degradation process of the dye molecules was further investigated after the dye molecules were adsorbed on the surface of RGO@ZnO.

3.4. Enhanced Photocatalytic Activity of RGO@ZnO. The photocatalytic degradation of RhB was further carried out to evaluate the photocatalytic performance of RGO@ZnO under simulated sunlight irradiation. Figure 5 shows the absorption of original RhB solution and the time dependent absorption spectra of RhB solutions during simulated sunlight irradiation in the presence of PVP-capped ZnO NPs and RGO@ZnO. Without the presence of a catalyst, the degradation of RhB was negligible under simulated sunlight irradiation.[30] In comparison, the degradation of RhB can be observed in the presence of PVP-capped ZnO NPs and was completed within 75 min (Figure 5a). In the presence of RGO@ZnO, the degradation of RhB was completed within a shorter time of 60 min (Figure 5b). Figure 5c shows the relative change of the absorption peak intensity as a function of irradiation time. To discount the adsorption effect of catalyst on the RhB dye molecules in the dark, the suspension was stirred for 1 h in the dark to achieve the adsorption and desorption equilibration before the photocatalytic activity test. Then the concentration of RhB suspension was measured and used as the original concentration C_0. The Y-axis was reported as C/C_0, where C_0 and C were the initial and actual concentration of RhB at different reaction times, respectively. It can be clearly seen in Figure 5a−-c that under the identical test conditions, the decrease of RhB concentration was faster and more prominent with RGO@ZnO than PVP-capped ZnO. One of the reasons is the difference in the absorption capacity. As shown in Figure 4a, RGO@ZnO showed much higher RhB adsorption capacity than PVP-capped ZnO. Therefore, RhB was adsorbed by RGO@ZnO more than by PVP-capped ZnO even before UV-induced degradation, resulting in a drastic rapid decrease in the RhB concentration as shown in Figure 5b. The other reason is that RGO@ZnO showed enhanced photocatalytic activity than PVP-capped ZnO NPs. As shown in Figure 5d, the $\ln(C_0/C)$ plot shows a linear relationship with the irradiation time which reveals that the photodegradation of the dye molecules went through a pseudo-first-order kinetic reaction.[31] The degradation of RhB dye molecules is almost negligible in the presence of RGO sheets.[8] Hence RGO@ZnO showed the enhanced photocatalytic activity compared to PVP-capped ZnO NPs because of the combination of RGO and PVP-capped ZnO NPs.

The enhanced photocatalytic performance of RGO@ZnO compared to neat PVP-capped ZnO NPs may be attributed to the interactions between RGO sheets and PVP-capped ZnO NPs.[8] RGO was reported to play an important role as the electron acceptor and transporter in the RGO/semiconductor composites due to its two-dimensional π-conjugation structure.[29] For the RGO@ZnO, the photoexcited electrons can be transferred from the conduction band of PVP-capped ZnO NPs to the conductive RGO nanosheets. Thus, RGO served as an acceptor of the photoexcited electrons from PVP-capped ZnO NPs. Those charge carriers were rapidly transferred on the 2D planar structure of the RGO nanosheets. In this way, the recombination of photogenerated electrons and holes was successfully suppressed, leaving more charge carriers to form reactive species, promoting the degradation of dyes.[31,32]

4. CONCLUSIONS

In summary, RGO@ZnO composite has been successfully fabricated as a pollutant adsorbent and photocatalyst, which combines a self-assembly deposition and in situ photoreduction procedure. In this method, PVP was used as the intermedium to assembly ZnO NPs on RGO surface, followed by a UV-photoreduction procedure to convert GO to be RGO due to the photocatalytic activity of ZnO NPs. By this method, a dense, stable and uniform loading of ZnO NPs was achieved on RGO surface. The RGO in the RGO@ZnO possessed great adsorptivity of RhB dye molecules and PVP-capped ZnO in the RGO@ZnO can degrade RhB under simulated sunlight irradiation. Therefore, the adsorption property of RGO@ZnO can be recovered using the photocatalytic activity of ZnO NPs under simulated sunlight irradiation. The cycling performance of RGO@ZnO for dye adsorption was achieved up to 99% over 4 cycles. The RGO@ZnO also demonstrated higher photocatalytic activity for degrading RhB than neat PVP-capped ZnO NPs under simulated sunlight irradiation. The recoverable adsorption property and enhanced photocatalytic activity of the RGO@ZnO may make the composite a

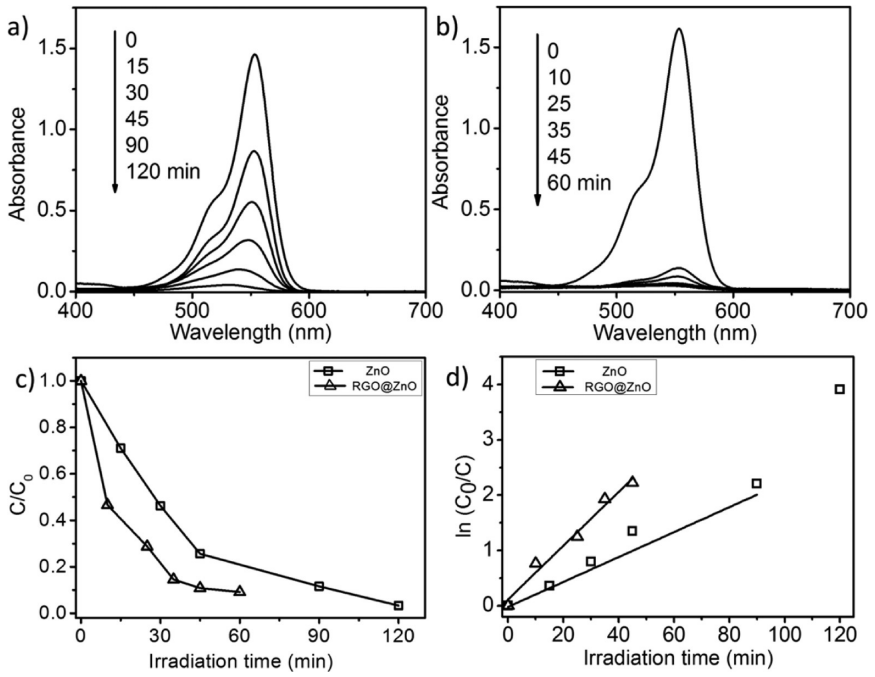

Figure 5. Time-dependent absorption spectra of RhB solutions during simulated sunlight irradiation in the presence of (a) PVP-capped ZnO NPs and (b) RGO@ZnO. Photocatalytic activity of (c) PVP-capped ZnO NPs and (d) RGO@ZnO as a function of irradiation time where C_0 and C are the initial and actual concentration of RhB at different reaction times, respectively.

promising material for practical applications in environmental pollutant management.

■ ASSOCIATED CONTENT

Ⓢ Supporting Information

TGA spectra of RGO@ZnO; the survey XPS spectra; the element atomic percentage; UV−vis absorption spectra; TEM image. This material is available free of charge via the Internet at http://pubs.acs.org.

■ AUTHOR INFORMATION

Corresponding Author

*E-mail: lu.sun@deakin.edu.au. Fax: +61 3 5227 2539. Tel: +61 3 5227 3247.

Notes

The authors declare no competing financial interest.

■ REFERENCES

(1) Srinivas, G.; Burress, J. W.; Ford, J.; Yildirim, T. *J. Mater. Chem.* **2011**, *21*, 11323−11329.
(2) Seredych, M.; Mabayoje, O.; Bandosz, T. J. *Langmuir* **2012**, *28*, 1337−1346.
(3) Seredych, M.; Mabayoje, O.; Bandosz, T. J. *J. Phys. Chem. C* **2012**, *116*, 2527−2535.
(4) Allen, M. J.; Tung, V. C.; Kaner, R. B. *Chem. Rev.* **2010**, *110*, 132−145.
(5) Xu, C.; Wang, X.; Zhu, J. *J. Phys. Chem. C* **2008**, *112*, 19841−19845.
(6) Muszynski, R.; Seger, B.; Kamat, P. V. *J. Phy. Chem. C* **2008**, *112*, 5263−5266.
(7) Li, B.; Cao, H.; Yin, J.; Wu, Y. A.; Warner, J. H. *J. Mater. Chem.* **2012**, *22*, 1876−1883.
(8) Li, B.; Cao, H. *J. Mater. Chem.* **2011**, *21*, 3346−3349.
(9) Wu, J.; Shen, X.; Jiang, L.; Wang, K.; Chen, K. *Appl. Surf. Sci.* **2010**, *256*, 2826−2830.
(10) Li, B.; Cao, H.; Yin, G.; Lu, Y.; Yin, J. *J. Mater. Chem.* **2011**, *21*, 10645−10648.
(11) Seredych, M.; Mabayoje, O.; Kolesnik, M. M.; Krstic, V.; Bandosz, T. J. *J. Mater. Chem.* **2012**, *22*, 7970−7978.
(12) Williams, G.; Kamat, P. V. *Langmuir* **2009**, *25*, 13869−13873.
(13) Williams, G.; Seger, B.; Kamat, P. V. *ACS Nano* **2008**, *2*, 1487−1491.
(14) Li, H.; Pang, S.; Wu, S.; Feng, X.; Müllen, K.; Bubeck, C. *J. Am. Chem. Soc.* **2011**, *133*, 9423−9429.
(15) Manga, K. K.; Zhou, Y.; Yan, Y.; Loh, K. P. *Adv. Funct. Mater.* **2009**, *19*, 3638−3643.
(16) Liu, X.; Pan, L.; Zhao, Q.; Lv, T.; Zhu, G.; Chen, T.; Lu, T.; Sun, Z.; Sun, C. *Chem. Eng. J.* **2012**, *183*, 238−243.
(17) Ng, Y. H.; Iwase, A.; Bell, N. J.; Kudo, A.; Amal, R. *Catal. Today* **2011**, *164*, 353−357.
(18) Ng, Y. H.; Iwase, A.; Kudo, A.; Amal, R. *J. Phys. Chem. Lett.* **2010**, *1*, 2607−2612.
(19) Yang, Y.; Ren, L.; Zhang, C.; Huang, S.; Liu, T. *ACS Appl. Mater. Interfaces* **2011**, *3*, 2779−2785.
(20) Pattanaik, M.; Bhaumik, S. K. *Mater. Lett.* **2000**, *44*, 352−360.
(21) Smith, J. N.; Meadows, J.; Williams, P. A. *Langmuir* **1996**, *12*, 3773−3778.
(22) Otsuka, H.; Esumi, K. *J. Colloid Interface Sci.* **1995**, *170*, 113−119.
(23) Hua, J.; Wang, Z.; Zhao, J.; Zhang, J.; Li, R.; Nie, H.; Sun, X. *Colloid Polym. Sci.* **2011**, *289*, 783−789.
(24) Hummers, W. S.; Offeman, R. E. *J. Am. Chem. Soc.* **1958**, *80*, 1339.
(25) Lambert, T. N.; Chavez, C. A.; Hernandez-Sanchez, B.; Lu, P.; Bell, N. S.; Ambrosini, A.; Friedman, T.; Boyle, T. J.; Wheeler, D. R.; Huber, D. L. *J. Phys. Chem. C* **2009**, *113*, 19812−19823.
(26) Wang, J.; Tsuzuki, T.; Tang, B.; Cizek, P.; Sun, L.; Wang, X. *Colloid Polym. Sci.* **2010**, *288*, 1705−1711.
(27) Zhang, J.; Shen, G.; Wang, W.; Zhou, X.; Guo, S. *J. Mater. Chem.* **2010**, *20*, 10824−10828.
(28) Pasricha, R.; Gupta, S.; Srivastava, A. K. *Small* **2009**, *5*, 2253−2259.
(29) Zhu, C.; Guo, S.; Wang, P.; Xing, L.; Fang, Y.; Zhai, Y.; Dong, S. *Chem. Commun.* **2010**, *46*, 7148−7150.
(30) Wang, Y.; Zhang, L.; Deng, K.; Chen, X.; Zou, Z. *J. Phys. Chem. C* **2007**, *111*, 2709−2714.

(31) Wan, Q.; Wang, T. H.; Zhao, J. C. *Appl. Phys. Lett.* **2005**, *87*, 083105.
(32) Zhang, H.; Lv, X.; Li, Y.; Wang, Y.; Li, J. *ACS Nano* **2009**, *4*, 380−386.